Journal of Organometallic Chemistry 694 (2009) 2866–2869

Contents lists available at ScienceDirect

Journal of Organometallic Chemistry

journal homepage: www.elsevier.com/locate/jorganchem

Note

Synthesis, crystal structure, magnetic properties and reactivity of a Ni–Ru model of NiFe hydrogenases with a pentacoordinated triplet (S = 1) Ni^{II} center

Yohan Oudart [a], Vincent Artero [a,*], Lucie Norel [b], Cyrille Train [b], Jacques Pécaut [c], Marc Fontecave [a]

[a] Laboratoire de Chimie et Biologie des Métaux, Université Joseph Fourier, CNRS, UMR 5249, CEA, DSV/iRTSV, 17 rue des Martyrs, F-38054 Grenoble Cedex 9, France
[b] Matériaux Magnétiques Moléculaires et Absorption X, Institut Parisien de Chimie Moléculaire, UMR 7201, UMPC Univ Paris 06, F 75252 Paris Cedex 05, France
[c] Laboratoire de Reconnaissance Ionique et Chimie de Coordination, UMR UJF/CEA-E3, 17 rue des Martyrs, F-38054 Grenoble Cedex 9, France

ARTICLE INFO

Article history:
Received 15 January 2009
Received in revised form 11 February 2009
Accepted 12 February 2009
Available online 28 February 2009

Keywords:
Hydrogen
Bio-inspired chemistry
Hydrogenases
High-spin complexes
Nickel
Ruthenium

ABSTRACT

The reaction of Ni(xbsms) (H_2xbsms = 1,2-bis(4-mercapto-3,3-dimethyl-2-thiabutyl)benzene) with [$Ru(CO)_3Cl_2$(thf)] yields green crystals of [NiCl(xbsms)$Ru(CO)_3$Cl]. The structure of this structural model of the active site of NiFe hydrogenase reveals a pentacoordinated nickel(II) center with bound chloride anion. It therefore adopts a paramagnetic (S = 1) electronic configuration as shown by magnetic susceptibility measurements. In DMF, this compound is converted into a red ionic-salt [NiL(xbsms)$Ru(CO)_3$Cl]Cl (L = water or DMF) that catalyzes hydrogen electro-evolution from Et_3NHCl at −1.52 V vs. Ag/AgCl (−2.05 V vs. $Fc^{0/+}$).

1. Introduction

Nickel–iron hydrogenases are metallo-enzymes that catalyze hydrogen evolution or oxidation [1]. Their active site consists of a nickel center coordinated, in a distorded geometry, by four cysteinate ligands, two of which bridge to an organometallic dicyanocarbonyl iron moiety (Chart 1). Electrochemical measurements carried out on hydrogenases adsorbed on carbon electrodes have shown that these enzymes are competitive to platinum as electrocatalysts [2]. Following a bio-inspired approach, it should thus be possible to design new catalysts for hydrogen evolution that contain only earth-abundant and cheap metal ions [3,4]. Nevertheless, despite a large number of reports on nickel–iron structural mimics, the sole dinuclear functional models so far are nickel–ruthenium compounds [5,6]. They indeed catalyze hydrogen electroproduction, probably via the formation of a bridging hydride derivative {Ni(μ-H)Ru}, the structure of which would reproduce that of the Ni–C state characterized along the enzymatic cycle of NiFe hydrogenases [7–9]. Here we report on a new member of this series, in which a $\{Ru(CO)_3Cl\}^+$ moiety is used as a surrogate for the $\{Fe(CN)_2CO\}$ fragment.

2. Results and discussion

The reaction of [$Ru(CO)_3Cl_2$(thf)] with [Ni(xbsms)] (H_2xbsms = 1,2-bis(4-mercapto-3,3-dimethyl-2-thiabutyl)benzene) in CH_2Cl_2 is complete within 5 min as evidenced by IR monitoring in the $\bar{\nu}$(CO) region. Then, the spectrum of the solution displays the A_1 + E pattern typical for fac-tricarbonyl coordination in octahedral complexes. Further crystallisation at 4 °C from a CH_2Cl_2/pentane mixture yields green crystals of [NiCl(xbsms)$Ru(CO)_3$Cl]. This compound, with maximum absorption wavelength at 698 nm in CH_2Cl_2, is paramagnetic as first evidenced by its ^{1}H NMR spectrum with broad signals up to 154 ppm. The ESI-MS spectrum displays one single peak corresponding to the $\{Ni(xbsms)Ru(CO)_3Cl\}^+$ fragment.

The crystal structure of [NiCl(xbsms)$Ru(CO)_3$Cl] is shown in Fig. 1. The two metal ions are involved in a $\{Ni(\mu\text{-}SR)_2M\}$ motif that mimics that found at the active site of NiFe hydrogenases (M = Fe). The distance between Ni and Ru is 3.316 Å. The main structural difference with the previously reported Ni–Ru complexes [5,6] regards the presence of an extra chloride ligand coordinated on the nickel center, here in a square-pyramidal environment. The nickel ion is slightly displaced from the 4S plane toward the chloride ligand. The ruthenium moiety is located trans to the axial methyl groups and therefore cis with the aromatic cycle of the xbsms ligand. A chloride ligand bound to ruthenium is directed towards but does not interact with the nickel atom (d(Cl···Ni) = 3.32 Å). Significant distortion in the equatorial plane of the ruthenium

* Corresponding author. Tel.: +33 438789106; fax: +33 438789124.
E-mail address: vincent.artero@cea.fr (V. Artero).

0022-328X/$ - see front matter © 2009 Elsevier B.V. All rights reserved.
doi:10.1016/j.jorganchem.2009.02.014

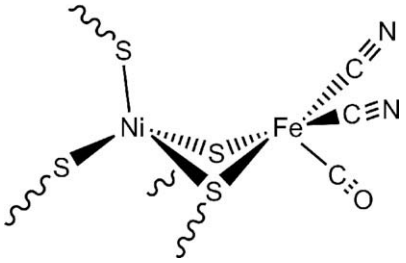

Chart 1. Structure of the active site of [NiFe] hydrogenases in the resting Ni–SI catalytically-active state.

octahedra arises from the acute S1–Ru–S4 angle (79.82(4)°) due to bridging constraints. The hinge angle defined by the S1–Ni–S4 and S1–Ru–S4 planes is 131.5°.

The ruthenium(II) ion (d^6 low-spin) is expected to be diamagnetic. Regarding the Ni(II) center, while low-spin electronic structure and diamagnetism is almost the rule for square-planar d^8 complexes [10], octahedral and square-pyramidal complexes can adopt a paramagnetic (S = 1) configuration [11] because of both the energetic degeneracy or proximity of the $d_{x^2-y^2}$ and d_{z^2} orbitals and the high pairing energy of these ions. Magnetic susceptibility measurements were recorded between 2 and 300 K and the χT versus T plot of data, corrected for diamagnetism and temperature-independent paramagnetism, is shown in Fig. 2. The room temperature value of χT is 1.2 cm^3 K mol^{-1} (3.1 Bohr magneton) in accordance with a high spin Ni(II) with average g value of 2.1–2.2. The shape of the curve shows that the high-spin state is maintained over the whole explored temperature range: the χT product does not vary significantly with temperature above 75 K but dramatically decreases at lower temperatures. Since there is no short contact between neighbouring complexes and the lowest Ni–Ni distance is 8.1 Å, this low temperature behavior shall be ascribed to the zero-field splitting (ZFS) generally encountered in distorted nickel(II) centers [12]. Accordingly the data were then fitted with a powder average value of $\chi = (1/3 \cdot \chi_{=} + 2\chi_{\perp})$, $\chi_{=}$ and $\chi_{\perp}$ being the axial and perpendicular magnetic susceptibility components intro-

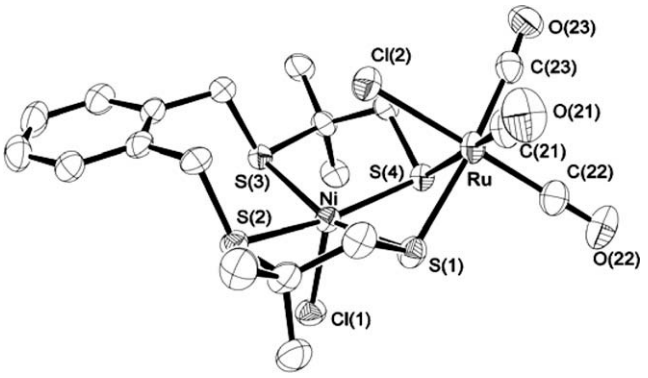

Fig. 1. Structure of [NiCl(xbsms)Ru(CO)$_3$Cl] in [NiCl(xbsms)Ru(CO)$_3$Cl] · 2CH_2Cl_2, crystallographic data are given in Tables S1 and S2). Selected bond lengths (Å) and angles (°): Ru–C(22) 1.901(5); Ru–C(21) 1.929(5); Ru–C(23) 1.947(5); Ru–Cl(2) 2.4166(12); Ru–S(4) 2.4302(11); Ru–S(1) 2.4389(12); Ni–Cl(1) 2.3141(13); Ni–S(4) 2.3520(12); Ni–S(1) 2.3681(12); Ni–S(2) 2.4108(12); Ni–S(3) 2.4259(13); O(21)–C(21) 1.128(6); O(22)–C(22) 1.123(6); O(23)–C(23) 1.122(5); C(22)–Ru–C(21) 93.0(2); C(22)–Ru–C(23) 93.37(19); C(21)–Ru–C(23) 96.22(19); C(22)–Ru–Cl(2) 179.16(15); C(21)–Ru–Cl(2) 86.86(15); C(23)–Ru–Cl(2) 87.47(13); C(22)–Ru–S(4) 90.78(14); C(21)–Ru–S(4) 171.70(14); C(23)–Ru–S(4) 90.90(13); Cl(2)–Ru–S(4) 89.20(4); C(22)–Ru–S(1) 89.56(15); C(21)–Ru–S(1) 92.85(15); C(23)–Ru–S(1) 170.31(12); Cl(2)–Ru–S(1) 89.61(4); S(4)–Ru–S(1) 79.82(4); Cl(1)–Ni–S(4) 101.97(5); Cl(1)–Ni–S(1) 103.09(5); S(4)–Ni–S(1) 82.88(4); Cl(1)–Ni–S(2) 93.81(5); S(4)–Ni–S(2) 163.40(4); S(1)–Ni–S(2) 88.59(4); Cl(1)–Ni–S(3) 93.69(4); S(4)–Ni–S(3) 88.29(4); S(1)–Ni–S(3) 162.32(4); S(2)–Ni–S(3) 95.89(4).

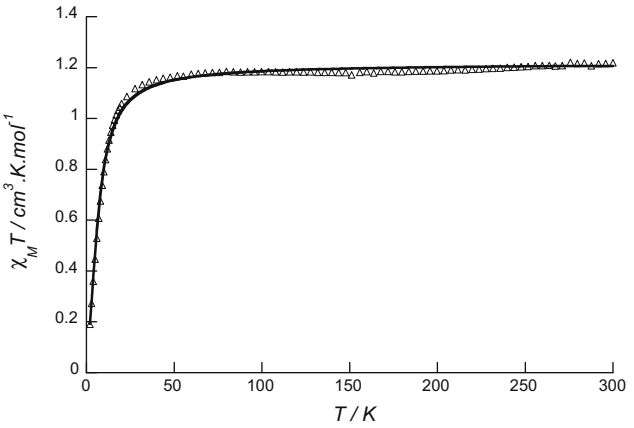

Fig. 2. Evolution of the χT product (dotted line: experimental, plain line: fitted curve), corrected for diamagnetism and temperature-independent paramagnetism, as a function of the temperature for a polycrystalline sample of [NiCl(xbsms)Ru(CO)$_3$Cl].

ducing the axial ZFS parameter D and the axial ($g_{=}$) and perpendicular ($g_{\perp}$) components of the g tensor. The simultaneous fit of χT (Fig. 2) and χ leads to the following values: D = 15 cm^{-1}, $g_{=}$ = 2.00 and $g_{\perp}$ = 2.07. The D value is among the highest observed for discrete nickel(II) complexes [13–16]. Since $g_{=}$ is lower than $g_{\perp}$, the magnetic susceptibility measurement also indicates that the ZFS parameter is positive [14] but further investigation by complementary methods [16], which are beyond the scope of the present paper, would be needed to ascertain this result.

The crop of green crystals is frequently contaminated by a red solid, with maximum absorption wavelength at 524 nm and the same ESI-MS spectrum. Dissolution of [NiCl(xbsms)Ru(CO)$_3$Cl] in a polar solvent such as CH_3CN or DMF irreversibly yields the same red compound. The nature of the solvent used has no clear influence on the UV–Vis or the ESI-MS spectrum. Its ^{1}H NMR spectrum displays broad signals constrained in the diamagnetic region, indicating for some dynamic solution equilibrium such as ligand exchange or stereochemical non-rigidity. We thus propose a ionic-salt structure [NiL(xbsms)Ru(CO)$_3$Cl]Cl, similar to that previously established for [Ni(xbsms)Ru(p-cymene)Cl]Cl but with an extra ligand L weakly coordinated on nickel (with L being water or any coordinating solvent molecule). Actually, from ^{1}H NMR and IR

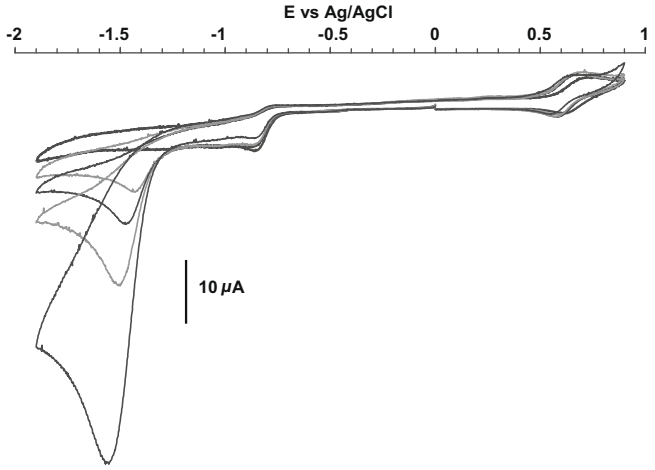

Fig. 3. Cyclic voltammograms of [NiL(xbsms)Ru(CO)$_3$Cl]Cl (1 mmol L^{-1}) in the presence of various amounts (0, 1.0, 1.5, 3.0 and 10 equiv.) of Et_3NHCl recorded in a DMF solution of n-Bu_4NBF_4 (0.1 mol L^{-1}) on a glassy carbon electrode at 100 mV s^{-1}.

measurements, this compound is the major species formed during the reaction of $[Ru(CO)_3Cl_2(thf)]$ with [Ni(xbsms)].

The cyclic voltamogram of $[NiL(xbsms)Ru(CO)_3Cl]Cl$ recorded on a glassy carbon electrode in DMF shows a reversible one-electron redox process at +0.68 V vs. Ag/AgCl and, on the cathodic counterpart, an irreversible monoelectronic reduction peak at −0.86 V vs. Ag/AgCl probably associated with the elimination of the chloride ligand from the ruthenium coordination sphere. Upon addition of Et_3NH^+ to this solution, a new irreversible cathodic wave appears at −1.52 V vs. Ag/AgCl (−2.05 V vs. $Fc^{0/+}$). It raises in height and shifts to more negative potentials when the acid/catalyst concentration ratio is increased as shown in Fig. 3 indicating an H_2-evolving electrocatalytic behavior similar to that observed for the previously reported Ni–Ru compounds. Hydrogen evolution, with 19 turnovers achieved within 4.5 h, is observed during the bulk electrolysis of 0.5 mmol of Et_3NHCl on a mercury pool at −1.60 V versus Ag/AgCl in DMF (10 mL) in the presence of 9 μmol of $[NiL(xbsms)Ru(CO)_3Cl]Cl$ as electrocatalyst. Under the same conditions but in the absence of catalyst, less than 5% of Et_3NH^+ is converted to H_2 within the same reaction time.

3. Conclusion

The nickel–ruthenium complex $[NiCl(xbsms)Ru(CO)_3Cl]$ is thus both a structural and functional mimic of NiFe hydrogenases. While most of the bio-inspired models reported so far contain a square-planar diamagnetic nickel(II) center, there is still a controversy based on L-edge X-ray absorption spectroscopy about the possibility for a high-spin nickel(II) center in the activated, EPR silent, Ni–SI resting state of native hydrogenases [17]. This compound is thus a valuable model for such a hypothesis, and the sole reported so far.

4. Experimental

4.1. Materials

All reactions were carried out in an argon atmosphere using Schlenk techniques. Solvents were dried using standard procedures and distillated under argon. NMR solvents were deoxygenated by three freeze-pump-thaw cycles and kept on molecular sieves. $[Ru(CO)_3Cl_2(thf)]$ [18] and [Ni(xbsms)] [19] were prepared according to reported procedures. Et_3NHCl (Acros) was used as received. The supporting electrolyte (n-$Bu_4N)BF_4$ was prepared from (n-$Bu_4N)HSO_4$ (Aldrich) and $NaBF_4$ (Aldrich) and dried overnight at 80 °C under vacuum.

4.2. Methods and instrumentation

^1H NMR spectra were recorded at room temperature in 5 mm *o.d.* tubes with a Bruker AC300 spectrometer equipped with a QNP probehead. Infrared spectra were recorded with a Bruker Vector 22 FTIR spectrophotometer; the spectra were recorded in solution, using a KBr cell. UV–Vis spectra have been recorded on a Carry Bio1 (Varian) spectrophotometer in quartz Schlenk cells. ESI-MS mass spectrometry was performed with a Finnigan LCQ thermoquest ion-trap. Elemental analyses were performed by the Service Central d'Analyse of the CNRS (Vernaison, France). Variable temperature magnetic data (2–300 K) were obtained with Quantum Design MPMS-XL squid magnetometer in a 0.2 T external field. The susceptibility was measured on a bench of single crystals (11.21 mg with less than 5% red crystals) and corrected for diamagnetism and temperature-independent paramagnetism on the basis of the slope s of the linear regime of the χT versus T plot at high temperature ($s = 5.5 \times 10^{-4}$ cm^3 mol^{-1}). All electrochemical measurements were carried out as previously reported [5,6,20,21] and potentials are quoted versus the Ag/AgCl/ KCl 3 mol L^{-1} reference electrode, abbreviated as Ag/AgCl. Using this reference electrode, the $(E_{pa} + E_{pc})/2$ value for the Fc/Fc^+ couple is measured in DMF at 0.55 V.

4.3. Synthesis

4.3.1. [NiCl(xbsms)Ru(CO)$_3$Cl]

$[Ru(CO)_3Cl_2(thf)]$ (126 mg, 0.38 mmol) and [Ni(xbsms)] (157 mg, 0.39 mmol) were dissolved in dichloromethane (5 mL) and stired for 30 min at room temperature. The solution is then evaporated in vacuum and the residue is dissolved in a CH_2Cl_2/pentane 1:1 mixture. Green crystals of $[NiCl(xbsms)Ru(CO)_3Cl] \cdot 2CH_2Cl_2$ (35 mg, 0.04 mmol, 10%), polluted with a small amount of red powder, are obtained upon cooling this solution for days at 4 °C. ^1H NMR (300 MHz, CD_2Cl_2): δ = 154, 33, 17, 10.1, 9.4, 7.4, 5.9, −1.7 ppm; UV–Vis (CH_2Cl_2): λ_{max} = 676 nm; ESI-MS (CH_2Cl_2) m/z (%) = 625 (100) $\{M-Cl\}^+$; IR (CH_2Cl_2): $\bar{\nu}_{CO} = 2124$(s), 2051 cm^{-1} (vs, broad); IR (KBr): $\bar{\nu}_{CO} = 2118$(s), 2056 cm^{-1} (s), 2046 cm^{-1} (s). Elemental Anal. Calc. for $C_{18}H_{26}S_4O_3NiRuCl_2$: C, 34.61; H, 3.67; Cl, 10.75. Found: C, 34.32; H, 3.77; Cl, 11.14%.

4.4. Crystal structure analysis

Crystallographic data are summarized in Table S1. Data collection was performed at 223 K by using a Bruker SMART diffractometer with a charged couple device area detector, with graphite-monochromated Mo Kα radiation (λ = 0.71073 Å). Empirical absorption correction (SADABS) was performed. Molecular structures were solved by direct methods and refined on F^2 by full-matrix least-squares techniques with the SHELXTL package [22] with anisotropic thermal parameters. All non-hydrogen atoms were refined anisotropically; hydrogen atoms were found and refined isotropically. The hydrogen atoms of the disordered solvent molecule were not introduced. The asymmetric unit contains one molecule and two CH_2Cl_2 molecules, one of which is disordered over two positions (with relative occupancies 0.598 and 0.402) around one C–Cl bond.

Acknowledgments

We thank the Life Science Division of the CEA for support within the BioHydrogen program and Colette Lebrun (CEA/DSM/INAC/SCIB/Laboratoire de Reconnaissance Ionique et Chimie de Coordination) for ESI-MS measurements.

Appendix A. Supplementary material

CCDC 712053 contains the supplementary crystallographic data for $[NiCl(xbsms)Ru(CO)_3Cl] \cdot 2\ CH_2Cl_2$. These data can be obtained free of charge from The Cambridge Crystallographic Data Centre via www.ccdc.cam.ac.uk/data_request/cif. Tables S1 and S2 provide additional crystallographic and structural informations. Supplementary data associated with this article can be found, in the online version, at doi:10.1016/j.jorganchem.2009.02.014.

References

[1] J.C. Fontecilla-Camps, A. Volbeda, C. Cavazza, Y. Nicolet, Chem. Rev. 107 (2007) 5411.
[2] A.K. Jones, E. Sillery, S.P.J. Albracht, F.A. Armstrong, Chem. Commun. (2002) 866.
[3] V. Artero, M. Fontecave, Coord. Chem. Rev. 249 (2005) 1518.
[4] S. Canaguier, V. Artero, M. Fontecave, Dalton Trans. (2008) 315.
[5] Y. Oudart, V. Artero, J. Pécaut, M. Fontecave, Inorg. Chem. 45 (2006) 4334.
[6] Y. Oudart, V. Artero, J. Pécaut, C. Lebrun, M. Fontecave, Eur. J. Inorg. Chem. (2007) 2613.

[7] S. Ogo, R. Kabe, K. Uehara, B. Kure, T. Nishimura, S.C. Menon, R. Harada, S. Fukuzumi, Y. Higuchi, T. Ohhara, T. Tamada, R. Kuroki, Science 316 (2007) 585.
[8] T.B. Rauchfuss, Science 316 (2007) 553.
[9] W. Lubitz, E. Reijerse, M. van Gastel, Chem. Rev. 107 (2007) 4331.
[10] A.J. Bridgeman, Dalton Trans. (2008) 1989.
[11] F. Pointillart, C. Train, F. Villain, C. Cartier dit Moulin, P. Gredin, L.M. Chamoreau, M. Gruselle, G. Aullon, S. Alvarez, M. Verdaguer, J. Am. Chem. Soc. 129 (2007) 1327.
[12] O. Kahn, Molecular Magnetism, VCH, Weinhem, 1993.
[13] P. Baltzer, A. Furrer, J. Hulliger, A. Stebler, Inorg. Chem. 27 (1988) 1543.
[14] R. Boca, Coord. Chem. Rev. 248 (2004) 757.
[15] H. Frydendahl, H. Toftlund, J. Becher, J.C. Dutton, K.S. Murray, L.F. Taylor, O.P. Anderson, E.R.T. Tiekink, Inorg. Chem. 34 (1995) 4467.
[16] J.N. Rebilly, G. Charron, E. Riviere, R. Guillot, A.L. Barra, M.D. Serrano, J. van Slageren, T. Mallah, Chem. Eur. J. 14 (2008) 1169.
[17] H.X. Wang, C.Y. Ralston, D.S. Patil, R.M. Jones, W. Gu, M. Verhagen, M. Adams, P. Ge, C. Riordan, C.A. Marganian, P. Mascharak, J. Kovacs, C.G. Miller, T.J. Collins, S. Brooker, P.D. Croucher, K. Wang, E.I. Stiefel, S.P. Cramer, J. Am. Chem. Soc. 122 (2000) 10544.
[18] M. Faure, L. Maurette, B. Donnadieu, G. Lavigne, Angew. Chem., Int. Ed. 38 (1999) 518.
[19] J.A.W. Verhagen, D.D. Ellis, M. Lutz, A.L. Spek, E. Bouwman, Dalton Trans. (2002) 1275.
[20] C. Baffert, V. Artero, M. Fontecave, Inorg. Chem. 46 (2007) 1817.
[21] M. Razavet, V. Artero, M. Fontecave, Inorg. Chem. 44 (2005) 4786.
[22] G.M. Sheldrick, SHELXTL 6.14, 5th ed., University of Göttingen, Göttingen, Germany, 2000.